Influence of a temperature-dependent shear viscosity on the azimuthal asymmetries of transverse momentum spectra in ultrarelativistic heavy-ion collisions

H. Niemi,[1,2] G. S. Denicol,[3] P. Huovinen,[3] E. Molnár,[2,4] and D. H. Rischke[2,3]

[1]*Department of Physics, P.O. Box 35 (YFL) FI-40014 University of Jyväskylä, Finland*

[2]*Frankfurt Institute for Advanced Studies, Ruth-Moufang-Str. 1, D-60438 Frankfurt am Main, Germany*

[3]*Institut für Theoretische Physik, Johann Wolfgang Goethe-Universität, Max-von-Laue-Str. 1, D-60438 Frankfurt am Main, Germany*

[4]*MTA Wigner Research Centre for Physics, H-1525 Budapest, P.O.Box 49, Hungary*

We study the influence of a temperature-dependent shear viscosity over entropy density ratio η/s, different shear relaxation times τ_π, as well as different initial conditions on the transverse momentum spectra of charged hadrons and identified particles. We investigate the azimuthal flow asymmetries as a function of both collision energy and centrality. The elliptic flow coefficient turns out to be dominated by the hadronic viscosity at RHIC energies. Only at higher collision energies the impact of the viscosity in the QGP phase is visible in the flow asymmetries. Nevertheless, the shear viscosity near the QCD transition region has the largest impact on the collective flow of the system. We also find that the centrality dependence of the elliptic flow is sensitive to the temperature dependence of η/s.

I. INTRODUCTION

Determining the properties of the quark-gluon plasma (QGP) is nowadays one of the most important goals in high-energy nuclear physics. For a system of weakly interacting particles reliable results can be obtained from first-principle quantum field-theoretical calculations. Unfortunately, for strongly interacting matter these tools provide only a limited amount of information. It is, however, possible to calculate the thermodynamical properties of such matter numerically from the theory of strong interactions, quantum chromodynamics (QCD). These lattice QCD calculations show that if the temperature is sufficiently high, the matter undergoes a transition from a confined phase where the relevant degrees of freedom are hadrons, to a deconfined phase where the degrees of freedom are quarks and gluons, the so-called QCD transition [1].

In recent years, experiments at the Relativistic Heavy-Ion Collider (RHIC) at Brookhaven National Laboratory [2] and the Large Hadron Collider (LHC) at CERN have provided a wealth of data from which one could in principle obtain information about the QGP. However, to compare these data with lattice QCD results is not straightforward. So far, lattice calculations have provided reliable results for static thermodynamical properties of QCD matter, e.g., the equation of state (EoS). The system created in heavy-ion collisions is, however, not static but dynamical, because it expands and cools in a very short time span of order 10^{-23} seconds. Obviously, in order to be able to properly interpret the experimental results and infer the properties of QCD matter, we also need a good understanding of the dynamics of heavy-ion collisions.

Fluid dynamics is one of the most commonly used frameworks to describe the space-time evolution of the created fireball, because the complicated microscopic dynamics of the matter is encoded in only a few macroscopic parameters like the EoS and the transport coefficients.

Currently, fluid-dynamical models give a reasonably good quantitative description of transverse momentum spectra of

hadrons and their centrality dependence [3–7]. So far, most calculations assume that the shear viscosity to entropy density ratio η/s is constant, and they show that, in order to describe the azimuthal asymmetries of the spectra, e.g., the elliptic flow coefficient v_2, this constant must be very small, of order 0.1. However, for real physical systems, η/s depends (at least) on the temperature [8]. A constant value of η/s can only be justified as an average over the space-time evolution of the system. It is not clear how this average is related to the temperature dependence of η/s.

In previous work [9,10], we have studied the consequences of relaxing the assumption of a constant η/s. We found that the relevant temperature region where the shear viscosity affects the elliptic flow most varies with the collision energy. At RHIC, the most relevant region is around and below the QCD transition temperature, while for higher collision energies the temperature region above the transition becomes more and more important. In this work we shall extend our previous study and provide a more detailed picture of the temperature regions that affect elliptic flow as well as higher harmonics at a given collision energy.

This paper is organized in the following way. In Sec. II, we describe our fluid-dynamical framework and its numerical implementation. In Sec. III, we specify the EoS, the transport coefficients, and the initialization. Sections IV and V contain a detailed compilation of our results, some of which were already shown in Refs. [9,10]. We present the transverse momentum spectra and the elliptic flow of hadrons at various centralities with different parametrizations of η/s as function of temperature. We also study the impact of different initial conditions and of the choice of the relaxation time for the shear-stress tensor. In Sec. VI, we investigate evolution of the elliptic flow in more detail and, in Sec. VII, find the temperature regions where v_2 and v_4 are most sensitive to the value of η/s. Finally, we summarize our results and give some conclusions. We use natural units $\hbar = c = k = 1$ throughout the paper.

II. FLUID DYNAMICS

A. Formalism

In order to describe the evolution of a system on length scales much larger than a typical microscopic scale, for instance the mean-free path, it is sufficient to characterize the state of matter by a few macroscopic fields, namely the energy-momentum tensor $T^{\mu\nu}$ and, possibly, some charge currents N_a^μ. Fluid dynamics is equivalent to the local conservation laws for these fields:

$$\partial_\mu T^{\mu\nu} = 0, \qquad \partial_\mu N_a^\mu = 0. \tag{1}$$

In the absence of conserved charges and bulk viscosity, the energy-momentum tensor $T^{\mu\nu}$ can be decomposed as

$$T^{\mu\nu} = e u^\mu u^\nu - P \Delta^{\mu\nu} + \pi^{\mu\nu}, \tag{2}$$

where $u^\mu = T^{\mu\nu} u_\nu / e$ is the fluid four-velocity, e is the energy density in the local rest frame of the fluid, i.e., in the frame where $u^\mu = (1, 0, 0, 0)$, and P is the thermodynamic pressure. The shear-stress tensor is defined as $\pi^{\mu\nu} = T^{\langle\mu\nu\rangle}$, where the angular brackets $\langle\rangle$ denote the symmetric and traceless part of the tensor orthogonal to the fluid velocity. With the $(+, -, -, -)$ convention for the metric tensor $g^{\mu\nu}$, the projector $\Delta^{\mu\nu} = g^{\mu\nu} - u^\mu u^\nu$.

If the system is sufficiently close to local thermodynamical equilibrium, the energy-momentum conservation equations can be closed by providing the EoS, $P(T)$, the equations determining $\pi^{\mu\nu}$, and the transport coefficients entering these equations, e.g., the shear viscosity $\eta(T)$. The EoS $P(T)$ and the shear viscosity $\eta(T)$ can in principle be computed by integrating out the dynamics on microscopic length scales.

While the conservation laws are exact for any system, the equations determining the shear-stress tensor require certain approximations, so that the only variables entering the equations of motion are those that appear in the energy-momentum tensor, namely e, u^μ, and $\pi^{\mu\nu}$. In the so-called relativistic Navier-Stokes approximation, the shear-stress tensor is directly proportional to the gradients of the four-velocity:

$$\pi^{\mu\nu} = 2\eta\sigma^{\mu\nu} \equiv 2\eta\partial^{\langle\mu} u^{\nu\rangle}. \tag{3}$$

We note that in this approximation the shear-stress tensor is not an independent dynamical variable.

Unfortunately, this approximation results in parabolic equations of motion, and subsequently the signal speed is not limited in this theory. In relativistic fluid dynamics this violation of causality leads to the existence of linearly unstable modes, which make relativistic Navier-Stokes (NS) theory useless for practical applications [11,12].

A commonly used approach that cures these instability and acausality problems is Israel-Stewart (IS) theory [13]. In this approach, the shear-stress tensor, the heat flow, and the bulk viscous pressure are introduced as independent dynamical variables and fulfill coupled, so-called relaxation-type differential equations of motion. Assuming vanishing heat-flow and bulk viscosity, the relaxation equation for the

shear-stress tensor can be written as [15]

$$\tau_\pi \dot\pi^{\langle\mu\nu\rangle} + \pi^{\mu\nu} = 2\eta\sigma^{\mu\nu} + \lambda_1 \pi^{\mu\nu}\theta + \lambda_2 \sigma^{\langle\mu}_{\ \alpha}\pi^{\nu\rangle\alpha}$$
$$+ \lambda_3 \pi^{\langle\mu}_{\ \alpha}\pi^{\nu\rangle\alpha} + \lambda_4 \omega^{\langle\mu}_{\ \alpha}\pi^{\nu\rangle\alpha}, \tag{4}$$

where $\dot A = u^\mu \partial_\mu A$ denotes the comoving derivative of A and $\theta = \partial_\mu u^\mu$ is the expansion scalar. The shear-relaxation time τ_π is the slowest time scale of the underlying microscopic theory [14]. Formally, IS theory can be derived by neglecting all faster microscopic time scales [15]. Like τ_π, the coefficients λ_i can in principle be calculated from the underlying microscopic theory, i.e., in our case QCD. Unfortunately, for QCD the transport coefficients appearing in Eq. (4) are still largely unknown. For the sake of simplicity, in this work we use $\lambda_1 = -4/3$, obtained from the Boltzmann equation for a massless gas [13], and $\lambda_2 = \lambda_3 = \lambda_4 = 0$. The shear-relaxation time and the shear viscosity are left as free parameters.

Instead of the full $(3+1)$–dimensional treatment, we consider a simplified evolution where the expansion in the z direction is described by boost-invariant scaling flow [16], i.e., the longitudinal velocity is given by $v_z = z/t$, and the scalar densities are independent of the space-time rapidity $\eta_s = \frac{1}{2}\log(\frac{t+z}{t-z})$. Here, t is the time measured in laboratory coordinates. In this approximation, the full evolution depends only on the coordinates (τ, x, y), where x and y are the transverse coordinates and $\tau = \sqrt{t^2 - z^2}$ is the longitudinal proper time.

B. Numerical implementation

Once the initial values of the components of the energy-momentum tensor are specified at a given initial time τ_0, the space-time evolution of the system is obtained by solving the conservation laws [Eq. (1)] together with the IS equations [Eq. (4)].

The conservation laws are solved using the algorithm developed in Refs. [17] and generalized to more than one dimension in Ref. [18]. This method, known as SHASTA for "sharp and smooth transport algorithm," solves equations of the type

$$\partial_t U + \partial_i (v_i U) = S(t, \mathbf{x}), \tag{5}$$

where $U = U(t, \mathbf{x})$ is, for example, T^{00}, T^{0i}, ..., v_i is the ith component of three-velocity, and $S(t, \mathbf{x})$ is a source term; for more details see Ref. [19].

We can further stabilize SHASTA by letting the antidiffusion coefficient A_{ad}, which controls the amount of numerical diffusion to be proportional to

$$\frac{1}{(k/e)^2 + 1}, \tag{6}$$

where e is the energy density in the local rest frame, and k is some constant of order 10^{-5} GeV/fm^3. In this way, A_{ad} goes smoothly to zero near the boundaries of the grid, i.e., we increase the amount of numerical diffusion in that region. We have checked that this neither affects the solution nor produces more entropy inside the decoupling surface.

The relaxation Eq. (4) could also be solved using SHASTA. However, we noticed that solving it by replacing the spatial

gradient at grid point i on the left-hand side of Eq. (4) by a centered second-order difference,

$$\partial_x U_i = \frac{U_{i+1} - U_{i-1}}{2\Delta x}, \tag{7}$$

where $U = \pi^{\mu\nu}$, yields a more stable algorithm. Time derivatives in the source terms are simply taken as first-order backward differences. Like in SHASTA, all spatial gradients in the source terms are discretized according to Eq. (7).

C. Freeze-out

We assume that freeze-out, i.e., the transition from the fluid-dynamical system to free-streaming particles happens on a hypersurface of constant temperature. Unless otherwise stated, we assume that the freeze-out temperature is $T_{\text{dec}} = 100$ MeV. We include all two- and three-particle decays of hadronic resonances according to Ref. [20].

The transverse momentum distribution of hadrons is calculated using the Cooper-Frye description [21]. For the final spectra we need to know the local single-particle momentum distribution functions of hadrons on the freeze-out surface. Here, we employ the widely used 14-moment ansatz where the correction to the local-equilibrium distribution $f_{0i} = \{\exp[(u_\mu p_i^\mu - \mu_i)/T] \pm 1\}^{-1}$ of a hadron of species i with four-momentum p_i^μ is given by [22]

$$\delta f_i = f_{0i} \frac{p_i^\mu p_i^\nu \pi_{\mu\nu}}{T^2 (e + P)}, \tag{8}$$

where $\pi^{\mu\nu}$ is the solution of Eq. (4). We note that this functional form for δf is merely an ansatz but consistent with Eq. (4). Other forms of δf are also possible, see, e.g., Ref. [23], and a full treatment of the multicomponent system further modifies δf; see Refs. [24,25]. Furthermore, if dissipative fluid dynamics is derived from the Boltzmann equation without assuming the 14-moment approximation, the full expansion of δf contains an infinite number of terms; for details see Ref. [15]. The effect of this will be studied in a future work.

III. PARAMETERS

A. Equation of state

As EoS we use the recent $s95p$-PCE-v1 parametrization of lattice QCD results [26]. In this parameterization, the high-temperature part is matched to recent results of the hotQCD collaboration [27,28] and smoothly connected to the low-temperature part described as a hadron resonance gas. All hadrons listed in Ref. [29] up to a mass of 2 GeV are included in the hadronic part of the EoS. The system is assumed to chemically freeze-out at $T_{\text{chem}} = 150$ MeV. Below this temperature the EoS is constructed according to Refs. [30–32]. This construction assumes that the evolution below T_{chem} is isentropic. Strictly speaking this is not the case in viscous hydrodynamics since dissipation causes an increase in entropy. However, we have checked that in our calculations the viscous entropy production from all fluid cells with temperatures below $T_{\text{chem}} = 150$ MeV is less than 1% of the initial entropy, whereas the entropy production during

the entire evolution ranges from 3 to 14%, depending on the collision energy and the η/s parametrization.

B. Transport coefficients

The temperature-dependent shear viscosity is parametrized as follows. In all cases, we take the minimum of η/s to be at $T_{\text{tr}} = 180$ MeV. Unless otherwise stated, the value of η/s at the minimum is assumed to equal the lower bound $\eta/s = 0.08$ conjectured in the framework of the AdS/CFT correspondence [34].

The parametrization of the hadronic viscosity is based on Ref. [35], where the authors consider a hadron resonance gas with additional Hagedorn states. In practice, we use a temperature dependence of η/s of the following functional form [9,36]:

$$\left. \frac{\eta}{s} \right|_{\text{HRG}} = 0.681 - 0.0594 \frac{T}{T_{\text{tr}}} - 0.544 \left(\frac{T}{T_{\text{tr}}} \right)^2. \tag{9}$$

At $T = 100$ MeV this coincides with the η/s value given in Ref. [35] and decreases smoothly to the minimum value $\eta/s = 0.08$ at T_{tr}. We note that many authors obtain considerably larger values for the shear viscosity of hadronic matter; see, e.g., Refs. [37]. Our motivation here is to illustrate the effects of hadronic viscosity rather than to use a parametrization that is as realistic as possible. We shall see that even this low η/s leads to considerable effects for hadronic observables in Au + Au collisions at RHIC. We further note that, since we are considering a chemically frozen hadron resonance gas below T_{chem}, while in Ref. [35] chemical equilibrium is assumed at all temperatures, the entropy densities, and therefore the values of η, differ between the two calculations at a given value of $T < T_{\text{chem}}$.

The high-temperature QGP viscosity is parametrized according to lattice QCD results [38] in such a way that it connects to the minimum of η/s at T_{tr}. The functional form used is

$$\left. \frac{\eta}{s} \right|_{\text{QGP}} = -0.289 + 0.288 \frac{T}{T_{\text{tr}}} + 0.0818 \left(\frac{T}{T_{\text{tr}}} \right)^2. \tag{10}$$

We take the following four parametrizations of the shear viscosity:

(1) (LH-LQ) $\eta/s = 0.08$ for all temperatures;
(2) (LH-HQ) $\eta/s = 0.08$ in the hadron gas, and above $T = 180$ MeV η/s increases according to Eq. (10);
(3) (HH-LQ) below $T = 180$ MeV, η/s is given by Eq. (9), and above we set $\eta/s = 0.08$;
(4) (HH-HQ) we use Eqs. (9) and (10) for the hadron gas and the QGP, respectively.

These parametrizations are shown in Fig. 1. Besides these four cases we also study the effect of varying the value of the minimum of η/s; see Secs. V and VII.

In order to complete the description, we also need to specify the relaxation time. In this work we use a functional form
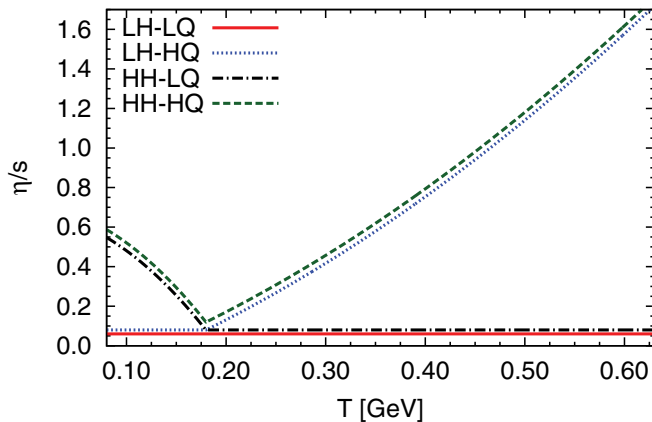
FIG. 1. (Color online) Different parametrizations of η/s as a function of temperature. The LH-LQ line is shifted downwards and the HH-HQ line upwards for better visibility.

suggested by kinetic theory,

$$\tau_\pi = c_\tau \frac{\eta}{e+p}, \quad (11)$$

where c_τ is a constant. Causality requires that $c_\tau \geqslant 2$ [12]. Unless otherwise stated, we shall use the value $c_\tau = 5$, which coincides with the value obtained from the Boltzmann equation in the 14-moment approximation for a massless gas of classical particles [39]. The relaxation times corresponding to the parametrizations above are shown in Fig. 2. The effect of varying the relaxation time separately from η is also studied in Sec. V.

C. Initial state

We still need to specify the initial state at some proper time τ_0. For a boost-invariant system it is sufficient to provide the components of the energy-momentum tensor in the transverse
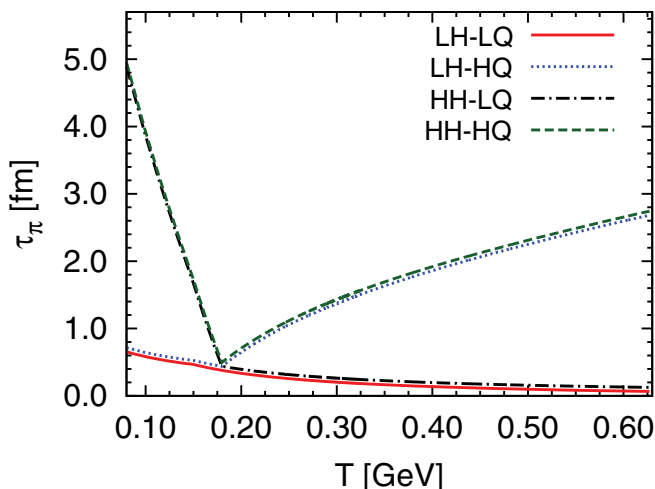
FIG. 2. (Color online) Relaxation times corresponding to the different parametrizations of η/s, for $c_\tau = 5$. The (LH-LQ) line is shifted downward and the (HH-HQ) line is shifted upward for better visibility.

plane at $z = 0$, i.e., $\eta_s = 0$. Within our approximations these are the local energy density, the initial transverse velocity, and the three independent components of the shear-stress tensor. Here, we will assume that the initial transverse velocity is zero and, unless otherwise stated, the initial shear-stress tensor is also assumed to be zero.

For the initial time we choose $\tau_0 = 1$ fm. The energy density $e(\tau_0, x, y)$ is based on the optical Glauber model by assuming that the energy density is a function of the density of binary nucleon-nucleon collisions n_{BC}, or the density of wounded nucleons n_{WN}, or both,

$$e(\tau_0, x, y) = C_e f(n_{BC}, n_{WN}). \quad (12)$$

The overall normalization, C_e, is fixed in order to reproduce the observed multiplicities in the most central $\sqrt{s_{NN}} = 200$ GeV Au + Au collisions at RHIC, and in $\sqrt{s_{NN}} = 2.76$ GeV Pb + Pb collisions at LHC.

The centrality dependence of the multiplicity is reproduced in this work in two different ways:

(1) BCfit: choosing f to be a polynomial in n_{BC},

$$f(n_{BC}) = n_{BC} + c_1 n_{BC}^2 + c_2 n_{BC}^3. \quad (13)$$

(2) GLmix: using a superposition of n_{BC} and n_{WN},

$$f(n_{BC}, n_{WN}) = d_1 n_{BC} + (1 - d_1) n_{WN}. \quad (14)$$

Here, the coefficient c_2 is introduced in order to guarantee that the parameterizations are monotonically increasing with increasing binary-collision or wounded-nucleon density. This ensures that the highest energy density is in the center of the system, i.e., at $x = y = 0$.

For a given impact parameter, the optical Glauber model yields a different number of participants and different central-ity classes than the Monte Carlo Glauber models commonly used by the experimental collaborations. Using the optical Glauber model, we can either choose to reproduce the multiplicity as a function of the number of participants or as a function of centrality classes. In general, this leads to different coefficients c_i and d_1. Here, we choose to determine the initial conditions by requiring that the centrality dependence of the charged particle multiplicity as a function of the number of participants [40,41] is reproduced. We have checked that, if we determine the centrality dependence by matching to the centrality classes given by the optical Glauber model, the elliptic flow is more suppressed in central and enhanced in peripheral collisions at RHIC energies, while at LHC energies it remains practically unchanged. In order to be fully consistent with the experimental determination of the centrality classes, one would need to generate fluctuating initial conditions via a Monte Carlo Glauber model; see, e.g., Refs. [42–44].

For $\sqrt{s_{NN}} = 5.5$ TeV Pb + Pb collisions we use the multiplicity in the most central collisions as predicted by the EKRT model [45]. In this case the centrality dependence is assumed to follow binary scaling, i.e., $c_1 = c_2 = 0$ in Eq. (13). All initialization parameters are shown in Table I.

Different parametrizations of η/s lead to different entropy production and therefore different final multiplicity, even if

TABLE I. Initialization parameters for different collision energies. The maximum temperature T_{max} is given for the BCfit initialization with the (LH-LQ) parameterization of η/s. For the other initializations T_{max} differs less than 5%.

$\sqrt{s_{NN}}$ [GeV]	c_1 [fm^{-2}]	c_2 [fm^{-4}]	d_1	T_{max} [MeV]
200	-0.032	0.00035	0.1	313
2760	-0.01	0.0001	0.7	430
5500	0	0	1.0	504

the initial state is kept the same. This is especially true for different parametrizations of the high-temperature shear viscosity, since most of the entropy is produced during the early stages of the collision [46]. We compensate this using different overall normalizations, e.g., between the (HH-LQ) and (HH-HQ) parametrizations. Entropy production during the hadronic evolution is small and not compensated. The centrality dependence of the entropy production is also different for different η/s parametrizations. Since it leads to at most a 5% difference in the final multiplicities and is hardly visible in the results, it is not corrected here.

IV. RESULTS AND COMPARISON WITH EXPERIMENTAL DATA

In this section we use the initializations and parametrizations of η/s given above and compare the results with experimental data from RHIC and LHC.

A. Transverse momentum spectra and elliptic flow at RHIC

In Fig. 3 we show the p_T-spectra of pions for different centrality classes for RHIC $\sqrt{s_{NN}} = 200$ GeV Au + Au collisions and compare them with PHENIX data [40]. We only show results using the BCfit initialization; those for the GLmix initialization are very similar. The freeze-out temperature is chosen as $T_{dec} = 100$ MeV. This choice reproduces the slopes of the p_T-spectra quite well.

Once we correct the normalization of the initial energy density profile for different entropy production (see discussion at the end of Sec. III C), the slopes of the p_T spectra are practically unaffected by the η/s parametrizations. We note that in our earlier work [9] this correction was not made, and the different η/s parametrizations lead not only to different multiplicities but also to different slopes for the p_T spectra. This effect was even more pronounced at LHC than at RHIC, due to an increase in entropy production caused by larger gradients appearing with an earlier initialization time $\tau_0 = 0.6$ fm.

The kaon spectra are shown in Fig. 4 and the proton spectra in Fig. 5 with the BCfit initialization. Both are compared with PHENIX data [40]. Because we do not consider net-baryon number in our calculations, the proton and antiproton spectra are identical. For this reason we show both the proton and the antiproton data in Fig. 5.

For both kaons and protons, the calculated spectra are slightly more curved than the data and they also lie above the
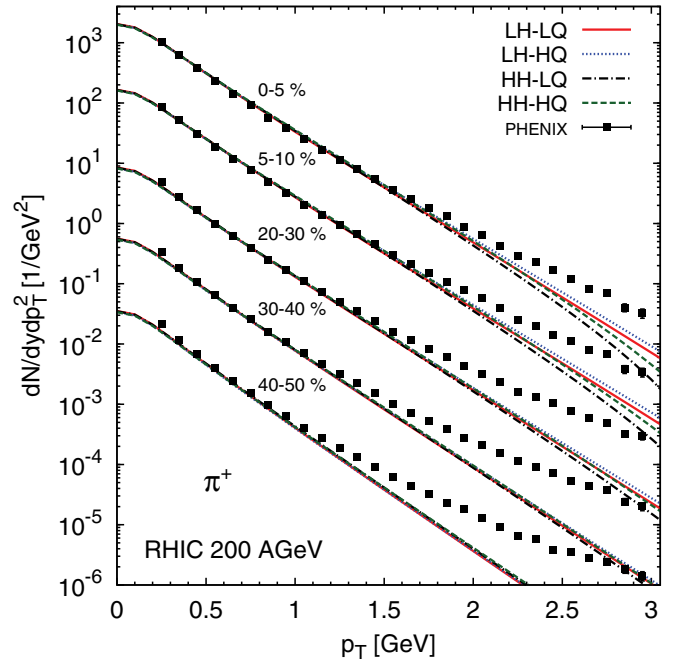

FIG. 3. (Color online) Pion spectra at RHIC, with BCfit initialization.

data. As for the pions, the slopes of the spectra are practically independent of the η/s parametrization.

Figure 6 shows the p_T-differential elliptic flow $v_2(p_T)$ of charged hadrons for different centrality classes using the BCfit initialization. Similarly, Fig. 7 shows the elliptic flow for the GLmix initialization. The calculations are compared with the four-particle cumulant data from the STAR collaboration [47].
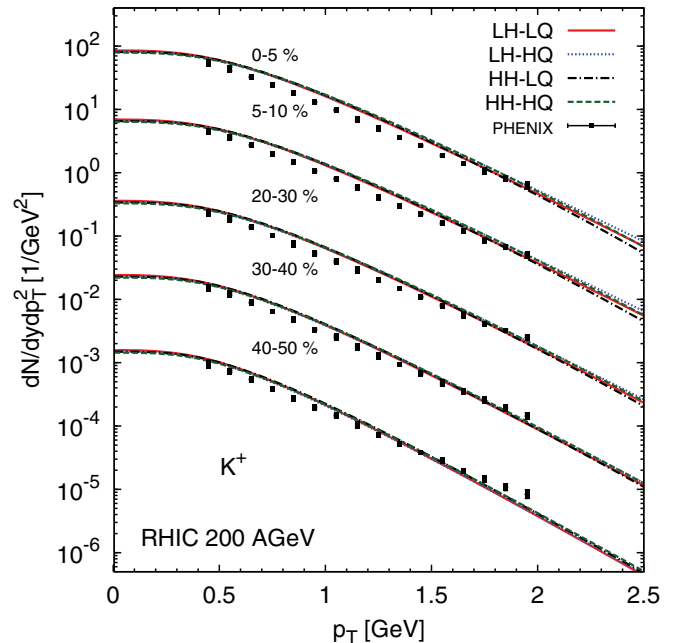

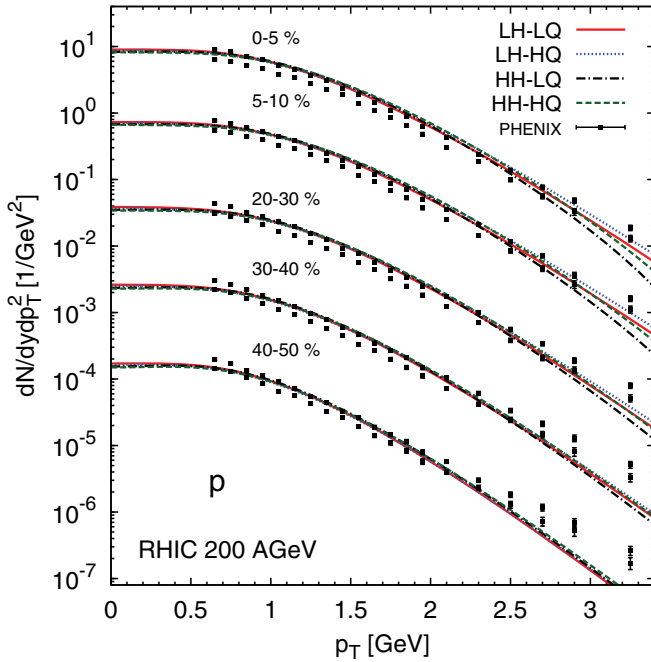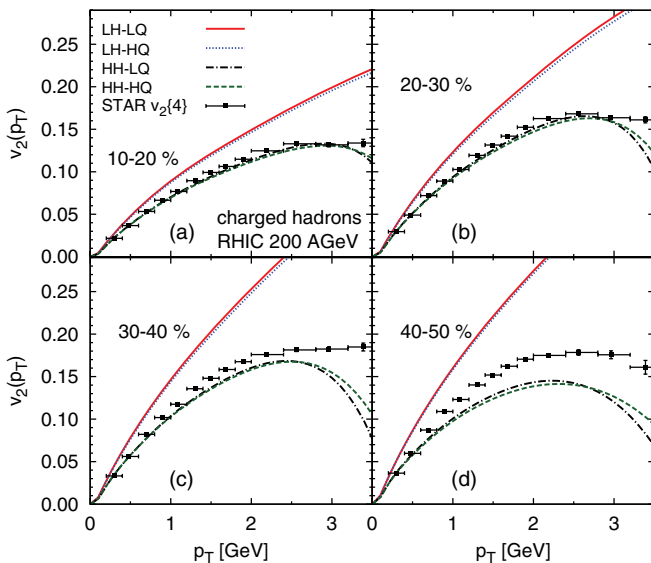FIG. 4. (Color online) Kaon spectra at RHIC, with BCfit initialization.

FIG. 5. (Color online) Proton spectra at RHIC, with BCfit initialization.

FIG. 7. (Color online) Charged hadron $v_2(p_T)$ at RHIC, with GLmix initialization.

As was observed in Ref. [9], the differential elliptic flow is largely independent of the high-temperature η/s parameterization, but highly sensitive on the hadronic η/s at RHIC. This holds for all centrality classes. The suppression of the elliptic flow due to the hadronic viscosity is even more enhanced in more peripheral collisions. Note that with the BCfit initialization, the elliptic flow in the most central collision class is reproduced by the parametrizations with a large hadronic viscosity, while with the GLmix initialization the elliptic flow in the same centrality class is better described by taking a constant $\eta/s = 0.08$. However, with the latter choice the

elliptic flow tends to be overestimated in more peripheral collisions. On the other hand, the temperature-dependent hadronic η/s gives the centrality dependence correctly down to the 30–40% centrality class. In even more peripheral collisions a large hadronic viscosity tends to suppress the elliptic flow too much.

Figure 8 shows $v_2(p_T)$ for protons with the BCfit initialization compared to the two-particle cumulant data from the STAR collaboration [48]. The protons show qualitatively the same response to the different η/s parametrizations as all charged hadrons, i.e., $v_2(p_T)$ depends strongly on the hadronic viscosity, but is almost independent of the high-temperature η/s. Since we use a smooth initialization, with no initial-state

FIG. 6. (Color online) Charged hadron $v_2(p_T)$ at RHIC, with BCfit initialization.
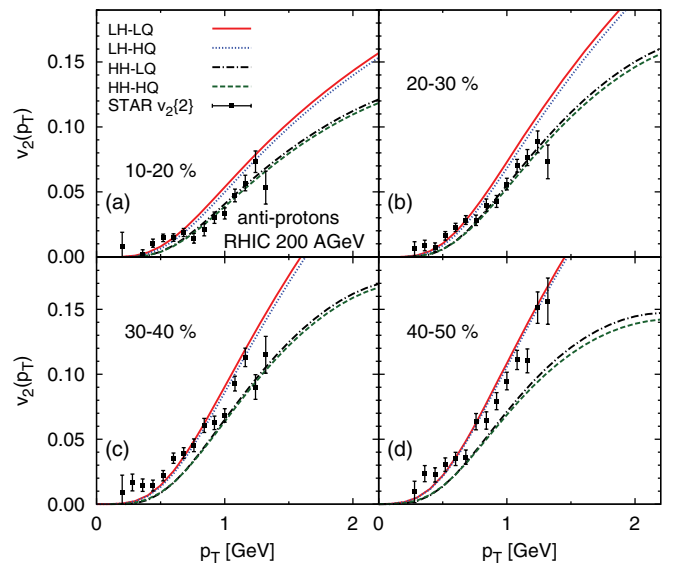

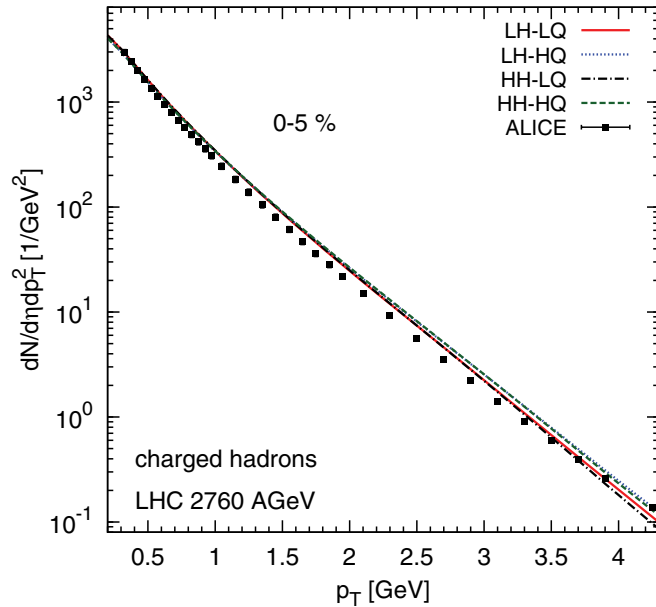FIG. 8. (Color online) Proton $v_2(p_T)$ at RHIC, with BCfit initialization.

FIG. 9. (Color online) Charged hadron spectra at LHC, with BCfit initialization.

fluctuations included, quantitative comparisons with two- or four-particle cumulant data are not straightforward.

B. Transverse momentum spectra and elliptic flow at LHC

Transverse momentum spectra of charged hadrons in most central Pb + Pb collisions with $\sqrt{s_{NN}} = 2.76$ TeV at LHC are shown in Fig. 9. At LHC, both initializations BCfit and GLmix give very similar results for both elliptic flow and the spectra, because the contribution from binary collisions is large, of order $\sim 70\%$; see Table I. Therefore, we show only results with the BCfit initialization; these are compared to data from the ALICE collaboration [49]. The calculated spectra are somewhat flatter than the data. Here, we have used the same decoupling temperature as at RHIC, i.e., $T_{\rm dec} = 100$ MeV. We could improve the agreement with the data by decoupling at even lower temperature than at RHIC. Another way to improve the agreement is choosing a larger chemical freeze-out temperature. This would give steeper spectra, but the proton multiplicity at RHIC would then be overestimated. However, we have tested that the dependence of the spectra and the elliptic flow on η/s is unchanged by these details.

As was the case at RHIC, at LHC the slopes of the spectra are practically independent of the η/s parametrization. We note that here we have used the initialization time $\tau_0 = 1.0$ fm, i.e., the same as at RHIC. In Ref. [9] we observed a quite visible correlation between the shear viscosity and the spectral slopes. Here, the later initialization time and the fact that we now compensate for the entropy production between different η/s parametrizations almost completely removes this correlation. However, the earlier the evolution starts, the more the viscosity will affect the slopes.

The p_T-differential elliptic flow for all charged hadrons is shown in Fig. 10 and for protons in Fig. 11. The charged hadron elliptic flow is compared with ALICE four-particle
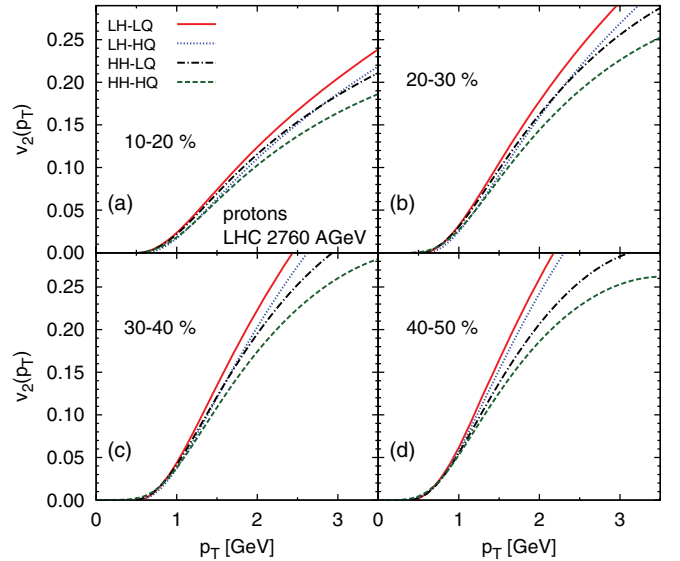

FIG. 10. (Color online) Charged hadron $v_2(p_T)$ at LHC, with BCfit initialization.

cumulant data [50]. We can see that in the 10–20% centrality class, changing the hadronic η/s or changing the high-temperature η/s has quite a similar impact on the elliptic flow; e.g., the difference between the LH-LQ and LH-HQ and between the LH-LQ and HH-LQ curves is nearly the same. However, the more peripheral the collision is, the more the viscous suppression is dominated by the hadronic η/s. This is confirmed by comparing the grouping of the flow curves in the 40–50% centrality class at LHC with that at RHIC; cf. Figs. 6 and 10. As was the case in Au + Au collisions at RHIC, also here the grouping of the curves for the protons is similar to that of all charged hadrons; cf. Fig. 11.

Note that, within our set-up, the best agreement with the ALICE data is obtained with the HH-HQ parametrization,
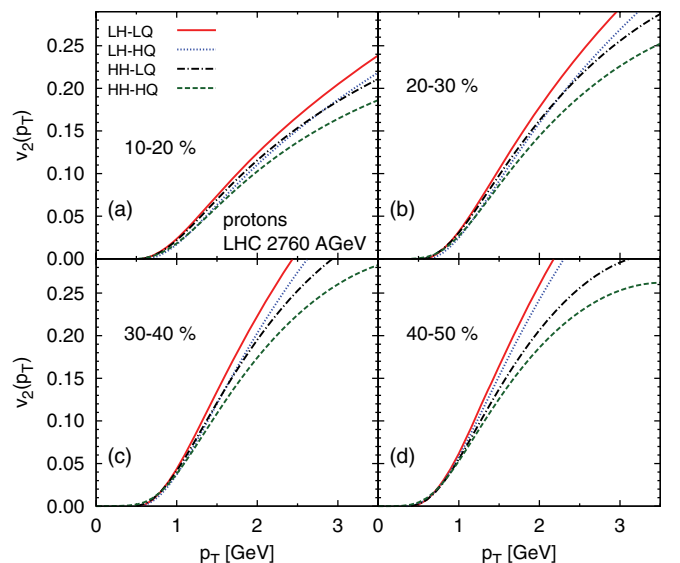

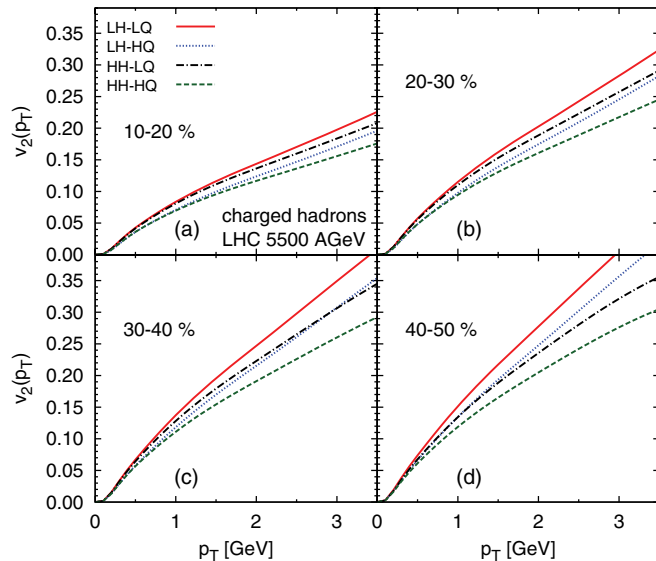FIG. 11. (Color online) Proton $v_2(p_T)$ at LHC, with BCfit initialization.

FIG. 12. (Color online) Charged hadron $v_2(p_T)$ at LHC 5.5 A TeV, with BC initialization.

i.e., with a temperature-dependent η/s in both hadronic and high-temperature phases. However, in the low-p_T region our calculations systematically underestimate the elliptic flow in all centrality classes. As was the case with the p_T spectrum, decoupling at a lower temperature and choosing a higher chemical freeze-out temperature would improve the agreement, without changing the grouping of the elliptic flow curves with the η/s parametrizations.

In Fig. 12 we show the p_T-differential elliptic flow for $\sqrt{s_{NN}} = 5.5$ TeV Pb + Pb collisions. In this case the viscous suppression of $v_2(p_T)$ is dominated by the high-temperature η/s in central collisions, while peripheral collisions resemble more the lower-energy central collisions at LHC; i.e., both hadronic and high-temperature viscosity contribute similarly to the suppression. Furthermore, the higher the p_T, the more the hadronic viscosity contributes to the suppression. This happens mainly because δf increases with both viscosity and p_T.

V. EFFECTS OF SHEAR INITIALIZATION, MINIMUM OF η/s AND RELAXATION TIME

One of the main results of Ref. [9] is that, at RHIC, the high-temperature shear viscosity has very little effect on the elliptic flow. In this section we elaborate more on this analysis and explicitly show that this statement holds for an out-of-equilibrium initialization of the shear-stress tensor as well. We also study the effect of varying the relaxation time.

Figure 13 shows the elliptic flow of charged hadrons in the 20–30% centrality class at RHIC. Instead of setting $\pi^{\mu\nu}$ to zero initially, here the so-called Navier-Stokes (NS) initialization where the initial values of the shear-stress tensor are given by the first-order, asymptotic solution of IS theory, Eq. (3). For all η/s parametrizations, the NS initialization increases the entropy production (up to 30%), especially for the parametrizations with a large high-temperature viscosity.
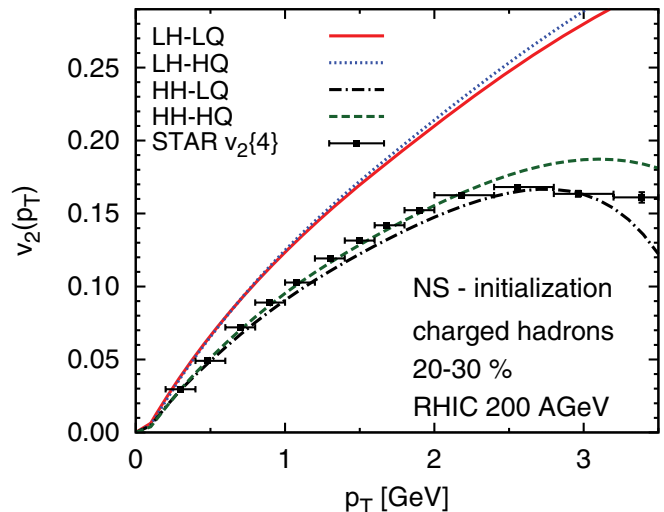

FIG. 13. (Color online) Charged hadron $v_2(p_T)$ at RHIC, with BCfit and NS initialization.

This is corrected by adjusting the initial energy density to produce approximately the same final multiplicity. Although for the parametrizations with a large hadronic η/s the different shear initializations give slightly different $v_2(p_T)$ curves, the grouping of these curves remains intact. We emphasize that the NS initialization gives very different initial conditions for each viscosity parametrization. If we use the same nonzero initial shear stress, e.g., $\pi^{\mu\nu} = \text{const.} \times \sigma^{\mu\nu}$, for each parametrization, the resulting $v_2(p_T)$ curves in each group in Fig. 13 would be even closer to each other.

The NS initialization with a constant $\eta/s = 0.08$ has a relatively short relaxation time; see Fig. 2. Hence, for $\tau_\pi \ll \tau_0$ the NS initialization is not a completely unrealistic assumption for the initial values of $\pi^{\mu\nu}$. However, for larger values of η/s the relaxation times are considerably larger, $\tau_\pi \gtrsim \tau_0$, and there is no reason to assume that the asymptotic solution could have been reached already at very early times.

So far we have changed the shear-viscosity parametrization by keeping the minimum fixed. In Fig. 14 we show the
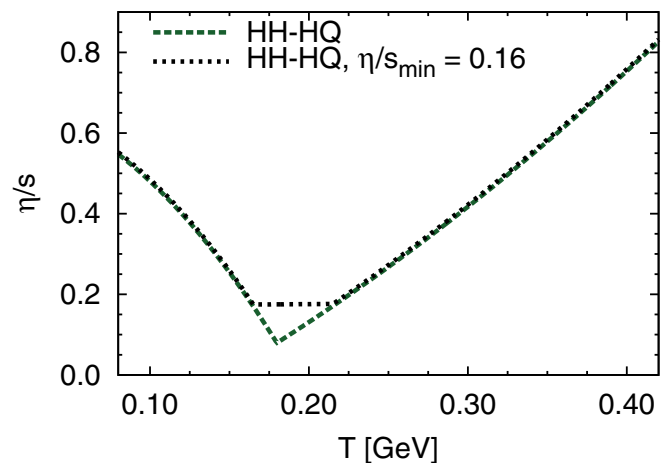

FIG. 14. (Color online) Parameterizations of η/s as a function of temperature. The (HH-HQ) line is the same as in Fig. 1.
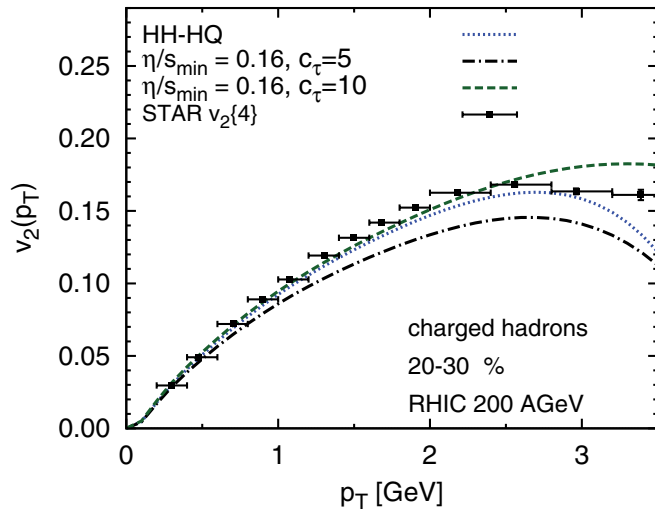
FIG. 15. (Color online) Charged hadron $v_2(p_T)$ at RHIC, with BCfit initialization and for different minima of η/s and relaxation times.

original HH-HQ parameterization and one where η/s around the minimum is twice as large. Figure 15 shows three $v_2(p_T)$ curves for Au + Au collisions at RHIC: one with the original HH-HQ parametrization, one with the larger minimum value of η/s, and the last one with the same large minimum value of η/s, but with a larger relaxation time; i.e., the constant in the relaxation time Eq. (11) is $c_\tau = 10$ instead of $c_\tau = 5$. We note that even a relatively small change in the η/s parameterization near the minimum produces quite a visible change in $v_2(p_T)$. At RHIC, this change can be almost completely compensated by adjusting the relaxation time. This shows that in small, rapidly expanding systems like the one formed in heavy-ion collisions, transient effects have considerable influence on the evolution. In other words, the relaxation time cannot be merely considered as a way to regularize the unstable Navier-Stokes theory: it has real physical effects that cannot be completely distinguished from the effects of η/s. In $\sqrt{s_{NN}} = 2.76$ TeV Pb + Pb collisions at LHC, the effect of changing the minimum or the relaxation time is practically the same.

VI. TIME EVOLUTION OF THE ELLIPTIC FLOW

One way to probe the effects of shear viscosity on the elliptic flow is to calculate the time evolution of the latter. Typically this is done by calculating the so-called momentum-space anisotropy from the energy-momentum tensor,

$$\varepsilon_p = \frac{\langle T^{xx} - T^{yy} \rangle}{\langle T^{xx} + T^{yy} \rangle}, \tag{15}$$

where the $\langle \cdots \rangle$ denotes the average over the transverse plane. The problem is, however, that one cannot make a direct connection of ε_p to the actual value of v_2 obtained from the decoupling procedure. Also, this way of studying the time evolution does not take into account that, at fixed time, part of the matter is already decoupled; i.e., the average over the transverse plane includes also matter that is outside the decoupling surface.
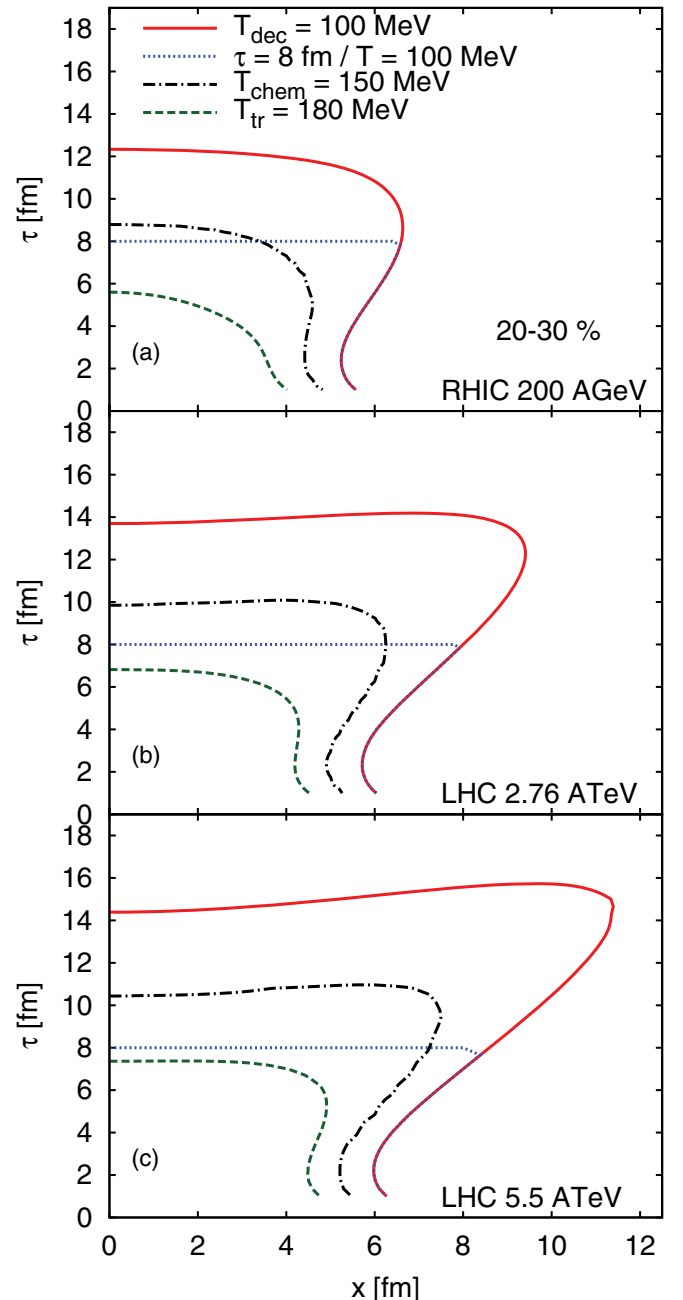

FIG. 16. (Color online) Constant-temperature hypersurfaces at decoupling ($T_{\text{dec}} = 100$ MeV), chemical freeze-out ($T_{\text{chem}} = 150$ MeV), and at the minimum of η/s ($T_{\text{tr}} = 180$ MeV) at different collision energies. Also, examples of surfaces that are used in the calculation of the time evolution of v_2 are shown (dotted lines).

To overcome these two shortcomings of ε_p, we instead calculate the v_2 of pions from a constant-time hypersurface that is connected smoothly to a constant-temperature hypersurface at the edge of the fireball; see Fig. 16 for examples of such hypersurfaces. Although the pions do not exist as real particles before hadronization, the advantage is that the final v_2 we obtain matches the one of thermal pions from the full decoupling calculation.
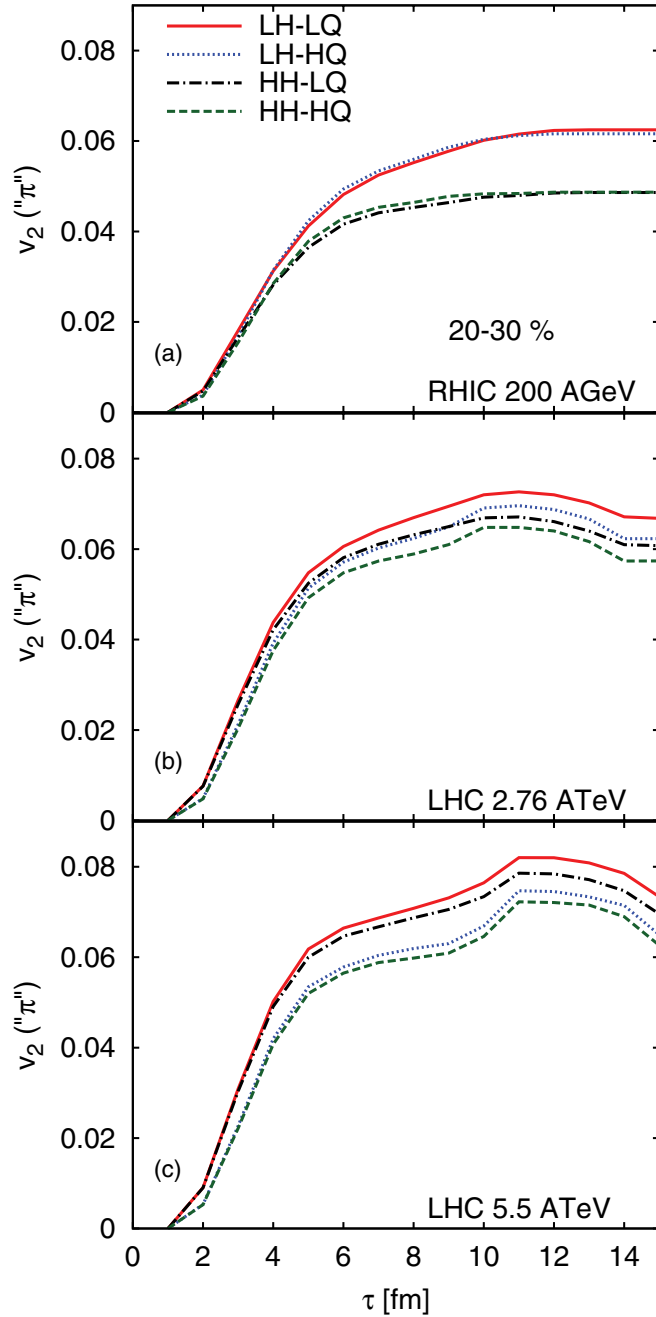
FIG. 17. (Color online) Time evolution of v_2 at different collision energies.
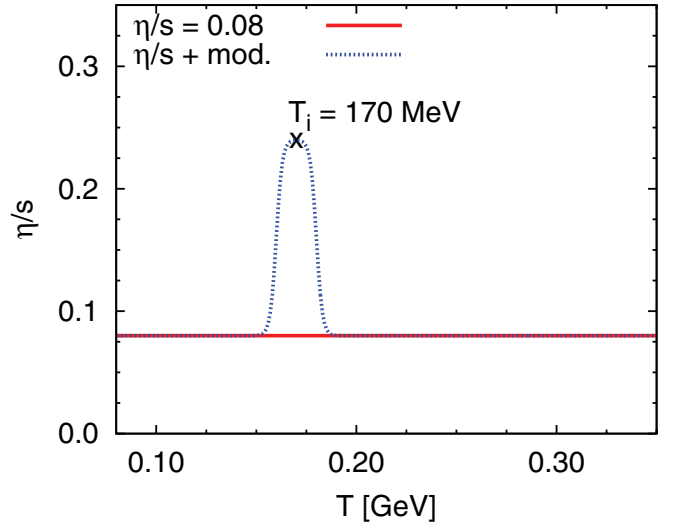

FIG. 18. (Color online) Shear viscosity with a modified temperature dependence.

viscosity. At the highest LHC energy the hadronic suppression is small and the effect of the QGP viscosity clearly dominates the grouping of the v_2 curves. Interestingly, both LHC evolutions show an increase of v_2 around $\tau = 10$ fm/c. This is when the system is going through the chemical decoupling stage. In the chemically frozen system, v_2 tends to increase more rapidly than in chemical equilibrium [32,33]. At RHIC, the chemical decoupling happens earlier, and also the hadronic suppression is stronger, and the increase in v_2 is washed out.
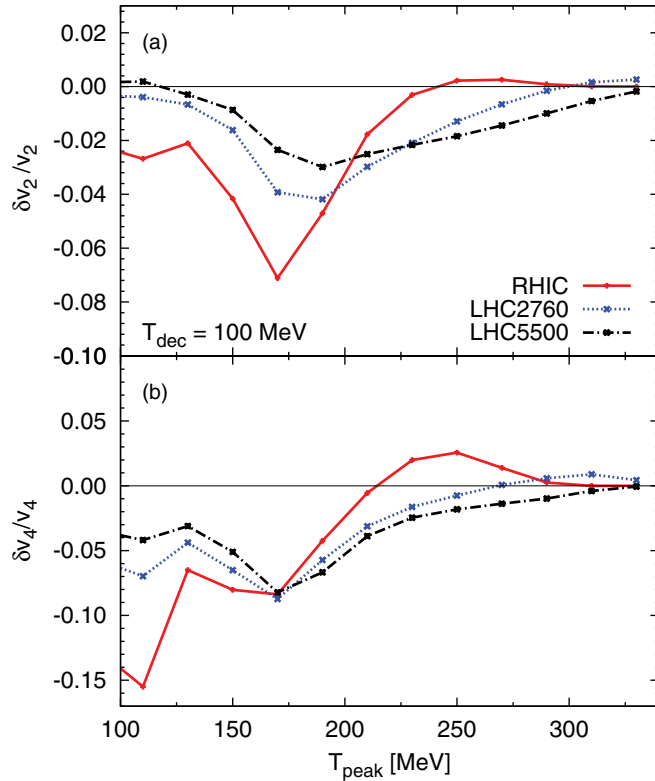
VII. PROBING THE EFFECTS OF A TEMPERATURE-DEPENDENT η/s ON THE v_n's

In this section, we try to probe the effects of a temperature-dependent η/s on the azimuthal asymmetries in a more detailed way. To this end, we introduce a modified η/s. Our baseline is a constant $\eta/s|_c = 0.08$ that we then modify near some temperature T_i according to

$$\frac{\eta}{s}(T) = \frac{\eta}{s}\bigg|_c \left\{ 1 + 2 \left[\exp\left(\frac{|T - T_i| - \delta T}{\Delta} \right) + 1 \right]^{-1} \right\}, \quad (16)$$

where the parameters are taken to be $\delta T = 10$ MeV and $\Delta = 1.5$ MeV. One example of this η/s parametrization is shown in Fig. 18. We note that, although we use smooth initial conditions from the optical Glauber model, we still get nonzero v_n for all even n. Although these are much smaller than the ones obtained with the fluctuations included, we can still probe the effects of viscosity on these coefficients. In general, one expects that the viscosity affects higher harmonics more than the elliptic flow [43,51]. By changing the temperature T_i and comparing the simulations with a constant η/s we can find the temperature regions where v_2 or v_4 are most sensitive to changes of η/s at different collision energies.

Figure 19 shows the results for v_2 and v_4 in the 20–30% centrality class for RHIC and for both LHC energies considered earlier. We plot the relative difference $\delta v_n / v_n$, where $\delta v_n = v_n[\eta/s(T)] - v_n(\eta/s|_c)$. Each point in the figure

Figure 17 shows the time evolution of v_2 in Au + Au collisions at RHIC, in $\sqrt{s_{NN}} = 2.76$ TeV Pb + Pb collisions at LHC, and in $\sqrt{s_{NN}} = 5.5$ TeV Pb + Pb collisions at LHC. In all cases, the evolution is calculated in the 20–30% centrality class. These results confirm our earlier conjecture: at RHIC, the different η/s parametrizations create very little difference in the elliptic flow in the early stages of the collision, while at later stages the suppression due to the hadronic viscosity takes over and groups the v_2 curves according to the hadronic viscosity. At the intermediate LHC energy the impact of the QGP viscosity is larger, and the final v_2 still has a memory of this difference. The hadronic viscosity has a similar impact on v_2 as the QGP

FIG. 19. (Color online) Effects of modified η/s on v_2 and v_4.

FIG. 20. (Color online) Same as Fig. 19 but without the δf contribution.

corresponds to a different calculation, with a different value of T_i in Eq. (16). Similarly, Fig. 20 shows the same result but without the δf contribution to the freeze-out.

The viscosity can affect v_n in two ways: by changing the space-time evolution of the integrated quantities like the energy density or by changing the local particle-distribution function at freeze-out. With our small baseline viscosity, the effect on the local distribution function is quickly washed out during the evolution below the temperature T_i. Therefore, in these simulations, in most of the temperature points, the change in η/s affects v_n through the space-time evolution, except at the lowest-temperature point $T_i = 110$ MeV, where the peak in η/s is close to the freeze-out temperature $T_{dec} = 100$ MeV. If we exclude the lowest temperature point in v_4 at RHIC, we can read off from the figures that the temperature region where viscosity affects both v_2 and v_4 most is around the transition region $T \sim 150 \ldots 200$ MeV. For v_2 this temperature region shifts slightly toward higher temperatures with increasing collision energy, while for v_4 the temperature where the effect is maximal is practically unchanged. Other than this, the overall behavior of v_2 and v_4 is quite similar. At high temperatures, the effect of η/s increases with increasing collision energy, while at low temperatures the viscous suppression decreases with increasing collision energy, which is most notable for the $T_i = 110$ MeV point where the viscosity effects on the freeze-out distribution are strongest.

For v_2 we observed earlier that the suppression due to the hadronic viscosity practically vanishes at the highest-energy LHC collisions. This is again confirmed in Fig. 19. This is, however, not true for higher harmonics. For v_4 there is still
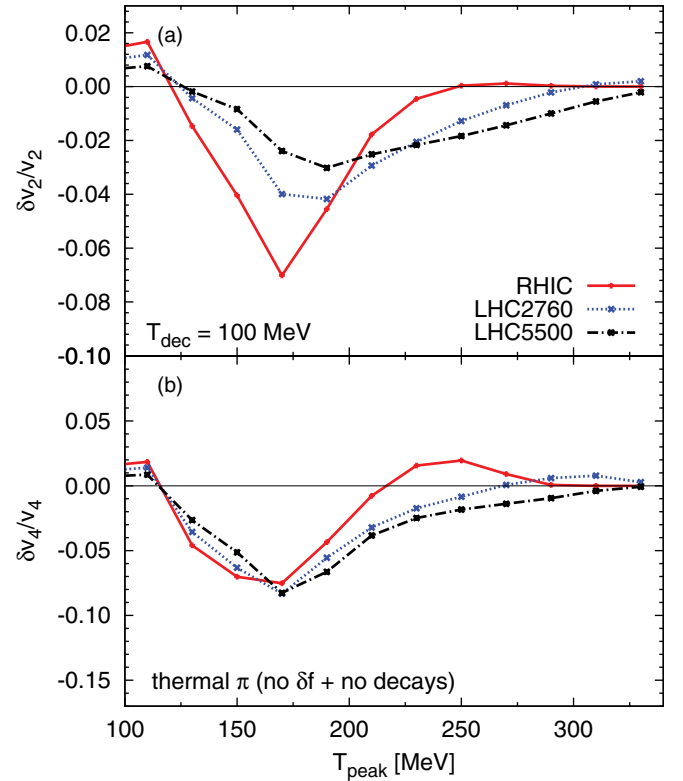
a significant contribution from hadronic viscosity at the full LHC energy. In this sense, higher harmonics do not give direct access to the high-temperature viscosity but can rather help in constraining the hadronic dynamics and viscosity as well as the correct form of δf. This is also important since the hadronic evolution always tends to shadow the effects of the properties of the high-temperature matter.

VIII. CONCLUSIONS

We have studied the effects of a temperature-dependent η/s on the azimuthal asymmetries of hadron transverse momentum spectra. We found earlier [9] that the viscous suppression of the elliptic flow is dominated by the hadronic viscosity in $\sqrt{s_{NN}} = 200$ GeV Au + Au collisions at RHIC, while in Pb + Pb collisions at the full LHC energy $\sqrt{s_{NN}} = 5.5$ TeV the suppression is mostly due to the high-temperature shear viscosity. In this work we have supplemented these earlier studies with more details.

First, we found that the suppression of the elliptic flow due to the shear viscosity becomes more important in more peripheral collisions. At least in our set-up, for RHIC energies a temperature-dependent shear viscosity improves the centrality dependence of the elliptic flow compared to the data, similarly to what was found in the hybrid approach of Ref. [5]. With a constant $\eta/s = 0.08$ and with the GLmix initialization, the measured $v_2(p_T)$ is reproduced in the most central collisions, but the calculations give a too large elliptic flow for peripheral collisions. However, with the BCfit initialization

the elliptic flow in the most central collisions is reproduced with a temperature-dependent viscosity and also the centrality dependence is reproduced down to the 30–40% centrality class. Similarly, in Pb + Pb collisions at LHC both a temperature-dependent hadronic η/s as well as an increasing η/s in the high-temperature phase help in reproducing the centrality dependence. Although there are lots of uncertainties associated with the decoupling and the initial state, at RHIC the centrality dependence of $v_2(p_T)$ may give access to the temperature dependence of η/s in hadronic matter.

Furthermore, we have studied the effects of a temperature-dependent η/s in a more detailed way. We found that for a given collision energy both v_2 and v_4 are most sensitive to the shear viscosity near the transition temperature, i.e., $T \sim$ 150–200 MeV. For v_2, this region moves slightly to higher temperature and widens with increasing collision energy, while for v_4 it remains practically unchanged. Other than that, the dependence of v_2 and v_4 on η/s is similar with increasing collision energy: the effect of the hadronic viscosity decreases and the effect of the high-temperature viscosity increases.

For v_2 the effect of δf almost vanishes at the highest collision energies, but for v_4 it always remains significant.

At RHIC the δf corrections clearly dominate v_4, and even at the highest collision energies this effect is comparable to the effects due to the modified space-time evolution. In this sense, higher harmonics give access to the δf corrections and the hadronic viscosity rather than the high-temperature viscosity.

ACKNOWLEDGMENTS

[1] P. Petreczky, Nucl. Phys., Proc. Suppl. **140**, 78 (2005); C. E. DeTar, PoS LATTICE **2008**, 001 (2008).

[2] I. Arsene *et al*., Nucl. Phys. A **757**, 1 (2005); B. B. Back *et al*., *ibid*. **757**, 28 (2005); J. Adams *et al*., *ibid*. **757**, 102 (2005); K. Adcox *et al*., *ibid*. **757**, 184 (2005).

[3] For a review, see, for instance, P. Huovinen and P. V. Ruuskanen, Annu. Rev. Nucl. Part. Sci. **56**, 163 (2006).

[4] P. Romatschke and U. Romatschke, Phys. Rev. Lett. **99**, 172301 (2007); M. Luzum and P. Romatschke, Phys. Rev. C **78**, 034915 (2008); P. Bozek, *ibid*. **81**, 034909 (2010); B. Schenke, J. Phys. G **38**, 124009 (2011); J. Peralta-Ramos and E. Calzetta, Phys. Rev. C **82**, 054905 (2010); T. Hirano, U. W. Heinz, D. Kharzeev, R. Lacey, and Y. Nara, *ibid*. **77**, 044909 (2008); Y. Hama, T. Kodama, and O. Socolowski Jr., Braz. J. Phys. **35**, 24 (2005).

[5] H. Song, S. A. Bass, U. Heinz, T. Hirano, and C. Shen, Phys. Rev. C **83**, 054910 (2011).

[6] C. Shen, U. Heinz, P. Huovinen, and H. Song, Phys. Rev. C **82**, 054904 (2010).

[7] H. Song, S. A. Bass, U. Heinz, T. Hirano, and C. Shen, Phys. Rev. Lett. **106**, 192301 (2011).

[8] L. P. Csernai, J. I. Kapusta, and L. D. McLerran, Phys. Rev. Lett. **97**, 152303 (2006).

[9] H. Niemi, G. S. Denicol, P. Huovinen, E. Molnar, and D. H. Rischke, Phys. Rev. Lett. **106**, 212302 (2011).

[10] H. Niemi, G. S. Denicol, P. Huovinen, E. Molnar, and D. H. Rischke, J. Phys. G **38**, 124050 (2011); Acta Phys. Polon. Supp. **5**, 305 (2012).

[11] W. A. Hiscock and L. Lindblom, Ann. Phys. (NY) **151**, 466 (1983); Phys. Rev. D **31**, 725 (1985); **35**, 3723 (1987); Phys. Lett. A **131**, 509 (1988); G. S. Denicol, T. Kodama, T. Koide, and Ph. Mota, J. Phys. G **35**, 115102 (2008).

[12] S. Pu, T. Koide, and D. H. Rischke, Phys. Rev. D **81**, 114039 (2010).

[13] W. Israel and J. M. Stewart, Proc. R. Soc. London A **365**, 43 (1979); Ann. Phys. **118**, 341 (1979).

[14] G. S. Denicol, J. Noronha, H. Niemi, and D. H. Rischke, Phys. Rev. D **83**, 074019 (2011); J. Phys. G **38**, 124177 (2011); G. S. Denicol, H. Niemi, J. Noronha, and D. H. Rischke, arXiv:1103.2476 [hep-th].

[15] G. S. Denicol, H. Niemi, E. Molnar, and D. H. Rischke, arXiv:1202.4551 [nucl-th].

[16] J. D. Bjorken, Phys. Rev. D **27**, 140 (1983).

[17] J. P. Boris and D. L. Book, J. Comp. Physiol. A **11**, 38 (1973); D. L. Book, J. P. Boris, and K. Hain, *ibid*. **18**, 248 (1975).

[18] S. T. Zalesak, J. Comp. Physiol. A **31**, 335 (1979).

[19] E. Molnar, H. Niemi, and D. H. Rischke, Eur. Phys. J. C **65**, 615 (2010).

[20] J. Sollfrank, P. Koch, and U. W. Heinz, Z. Phys. C **52**, 593 (1991).

[21] F. Cooper and G. Frye, Phys. Rev. D **10**, 186 (1974).

[22] D. Teaney, Phys. Rev. C **68**, 034913 (2003).

[23] K. Dusling, G. D. Moore, and D. Teaney, Phys. Rev. C **81**, 034907 (2010).

[24] A. Monnai and T. Hirano, Nucl. Phys. A **847**, 283 (2010).

[25] D. Molnar, J. Phys. G **38**, 124173 (2011).

[26] P. Huovinen and P. Petreczky, Nucl. Phys. A **837**, 26 (2010).

[27] M. Cheng *et al*., Phys. Rev. D **77**, 014511 (2008).

[28] A. Bazavov *et al*., Phys. Rev. D **80**, 014504 (2009).

[29] S. Eidelman *et al*. (Particle Data Group Collaboration), Phys. Lett. B **592**, 1 (2004).

[30] H. Bebie, P. Gerber, J. L. Goity, and H. Leutwyler, Nucl. Phys. B **378**, 95 (1992).

[31] T. Hirano and K. Tsuda, Phys. Rev. C **66**, 054905 (2002).

[32] P. Huovinen, Eur. Phys. J. A **37**, 121 (2008).

[33] T. Hirano and M. Gyulassy, Nucl. Phys. A **769**, 71 (2006).

[34] P. K. Kovtun, D. T. Son, and A. O. Starinets, Phys. Rev. Lett. **94**, 111601 (2005).

[35] J. Noronha-Hostler, J. Noronha, and C. Greiner, Phys. Rev. Lett. **103**, 172302 (2009); C. Greiner, J. Noronha-Hostler, and J. Noronha, arXiv:1105.1756 [nucl-th].

[36] G. S. Denicol, T. Kodama, and T. Koide, J. Phys. G **37**, 094040 (2010).

[37] K. Itakura, O. Morimatsu, and H. Otomo, Phys. Rev. D **77**, 014014 (2008); M. I. Gorenstein, M. Hauer, and O. N. Moroz, Phys. Rev. C **77**, 024911 (2008); N. Demir and S. A. Bass, Phys. Rev. Lett. **102**, 172302 (2009).

[38] A. Nakamura and S. Sakai, Phys. Rev. Lett. **94**, 072305 (2005).

[39] G. S. Denicol, T. Koide, and D. H. Rischke, Phys. Rev. Lett. **105**, 162501 (2010).

[40] S. S. Adler *et al*. (PHENIX Collaboration), Phys. Rev. C **69**, 034909 (2004).

[41] K. Aamodt *et al*. (ALICE Collaboration), Phys. Rev. Lett. **106**, 032301 (2011).

[42] H. Holopainen, H. Niemi, and K. J. Eskola, Phys. Rev. C **83**, 034901 (2011).

[43] B. Schenke, S. Jeon, and C. Gale, Phys. Rev. C **85**, 024901 (2012).

[44] Z. Qiu, C. Shen, and U. Heinz, Phys. Lett. B **707**, 151 (2012)

[45] K. J. Eskola, H. Honkanen, H. Niemi, P. V. Ruuskanen, and S. S. Räsänen, Phys. Rev. C **72**, 044904 (2005).

[46] A. Dumitru, E. Molnar, and Y. Nara, Phys. Rev. C **76**, 024910 (2007).

[47] Y. Bai, Ph.D. Thesis, Nikhef and Utrecht University (2007); A. Tang (STAR Collaboration), arXiv:0808.2144 [nucl-ex].

[48] J. Adams *et al*. (STAR Collaboration), Phys. Rev. C **72**, 014904 (2005).

[49] K. Aamodt *et al*. (ALICE Collaboration), Phys. Lett. B **696**, 30 (2011).

[50] K. Aamodt *et al*. (The ALICE Collaboration), Phys. Rev. Lett. **105**, 252302 (2010).

[51] B. H. Alver, C. Gombeaud, M. Luzum, and J.-Y. Ollitrault, Phys. Rev. C **82**, 034913 (2010).